Available online at www.sciencedirect.com
ScienceDirect
Trans. Nonferrous Met. Soc. China 22(2012) 1794−1800
Transactions of Nonferrous Metals Society of China
www.tnmsc.cn

Occurrence of lead and silver minerals and their interaction with xanthate in slurry of zinc electrolysis anode slime

XIANG Ping[1,2], FENG Qi-ming[1], ZHU Yang-ge[1], DENG Jie[1], LONG Tao[1], NIU Yin-jian[1]

1. School of Minerals Processing and Bioengineering, Central South University, Changsha 410083, China;
2. Xiangqi Research Institute for Comprehensive Utilization of Mineral Resources, Zhuzhou 412005, China

Received 25 July 2011; accepted 10 January 2012

Abstract: The background pulp potential of zinc anode slime, and its influence on the occurrence of lead, silver and xanthate, were investigated with thermodynamic method. The thermodynamic conclusion and XRD analysis pointed out that in zinc anode slime, the thermodynamically stable compound of xanthate is dixanthogen, anglesite is the only mineral of lead, and kerargyrite is one of silver minerals occurring. Microflotation tests on single minerals of anglesite and kerargyrite in sulfuric acid solution by amyl dixanthogen indicated that dixanthogen has a much stronger collecting ability to kerargyrite than to anglesite. Molecular dynamic simulation indicated that amyl dixanthogen can only be adsorbed on the surface of kerargyrite in the presence of SO_4^{2-}. The FTIR tests also verified the selective adsorption of amyl dixanthogen on the surface of kerargyrite in the presence of SO_4^{2-}.
Key words: zinc electrolysis anode slime; anglesite; kerargyrite; xanthate; adsorption

1 Introduction

In the anode slime resulting from the electrowinning of zinc, there are varying amounts of manganese, lead, and silver etc, depending upon the source of the anode. Some researchers reported that in zinc electrolysis anode slime, pyrolusite (MnO_2) occurred as the major manganese mineral [1,2]. Others regarded $PbSO_4$ or PbO_2 as the main lead minerals [3]. However, very little literature reported the occurrence of sliver in zinc anode slime.

φ−pH diagrams, also called Pourbaix diagrams or electrochemical phase diagrams, are useful tool for visualizing the stability areas of mineral or metal species in a solution depending on the solution's redox potential (φ) and pH. The location of predominance regions for typical species in these diagrams, or the occurrence of metal under different conditions of pulp potential, ion concentration or pH, can be predicted in advance. Many scholars reported their research on constructing φ−pH diagrams for variable metal−H_2O system to discuss the stable areas of metal species [4−7]. While, literatures that dealt with the φ−pH diagrams for Mn−H_2O systems to examine the background potential of zinc electrolysis anode slime caused from Mn(IV), and dealt with the influence of this background potential on the occurrence of lead and silver, and thiol collectors, were seldom.

Flotation by thiol collectors such as xanthate or aerofloat is a useful way to recover anglesite [8−10] and silver minerals [11,12] from hydrometallurgical smelting residues. However, literatures about the flotation recovery of anglesite and silver minerals from zinc anode slime by thiol collectors were also seldom. Several hydrometallurgical methods such as reductive roasting using coal as the reductant followed by sulfuric leaching [13], directly reductive acid leaching using zinc sulfide [14], lead sulfide [15], sulfur dioxide [16], or sulfuric acid hydrolysis of corn pole [17] as the reductant, had been proposed to treat the zinc anode slime by changing Mn(IV) to Mn(II) firstly, then dissolving Mn(II) into solution, and leaving the lead and silver in the solid residue. This hydrometallurgical methods had done well to recover valuable materials of lead and silver from the anode slime, but failed to separate Mn(IV) therefrom without changing the valence of manganese. Recently, we have reported a physical ore dressing method to treat zinc anode slime to realize the separation of manganese, lead and silver each other by not changing Mn(IV) to Mn(II) [18]. In this new technology, flotation was used

Foundation item: Project (51174229) supported by the National Natural Science Foundation of China
Corresponding author: FENG Qi-ming; Tel/Fax: +86-731-88836817; E-mail: qmfeng@csu.edu.cn
DOI: 10.1016/S1003-6326(11)61389-7

firstly to recover sliver from the zinc anode slime, followed by gravity separation using a shaking table together with magnetic separation using a high gradient magnetic separator to realize the sorting of anglesite from Mn(IV) mineral. The aims of this work are to investigate the pulp potential of the zinc electrolysis anode slime slurry in acid solution, to discuss its influence on the occurrence of xanthate and lead or silver minerals, and to research the adsorption of xanthate on the surface of lead and silver minerals in the pulp of zinc anode slime.

2 Experimental

2.1 Materials

The samples of anglesite and kerargyrite used in this study were A.R. grade lead sulphate and A.R. grade silver chloride, respectively. The samples were ground in a three-agate mortar vibration mill and sieved to a particle size of 37−75 um. Then, those processed samples were sealed in polyethylene bags to avoid cross-contamination. Commercial grade potassium amyl xanthate (KAX, purity>90%) was obtained from Zhuzhou Flotation Reagent Company, China. The amyl dixanthogen used was the oxidized product of KAX. 10 g of KAX was added into a beaker filled with 200 mL distilled water, then 50 mL of A.R. grade hydrogen peroxide (30% concentration) was poured into the solution in this collector. After 5 min of agitation, some water-insoluble oily liquid was found to be generated. This water-insoluble oily liquid was the oxidized product of KAX (amyl dixanthogen) and was separated from the solution by a separatory funnel. H_2SO_4−K_2SO_4 buffer system was used as pH buffer solution.

The sample of zinc electrolysis anode slime was taken from Zhuzhou Smelter Group Co., Ltd., China. The chemical composition of this sample is 33.79% Mn, 18.73% Pb, 1.84% Zn, 1.37% Sr, 6.42% S, 0.83% Ca, 1.83% K, 0.92% Na, 0.15% Fe and 0.176% Ag. Based on the XRD analysis, the major phases of this slime were cryptomelane (KMn_8O_{16}) and anglesite($PbSO_4$).

2.2 Microflotation tests

The microflotation tests for pure minerals of anglesite and kerargyrite were conducted in a XFG5−35 model hanging cell flotation machine. In each of the experiments in the absence of manganese dioxide, 2 g anglesite or kerargyrite sample was added into the flotation cell, then 30 mL of distilled water and a certain volume of pH buffer solution were added. After the pulp was conditioned for 5 min, the pH value of the slurry was measured using a PHS−25 model digital pH meter. And then potassium amyl xanthate was added to the slurry and the slurry was conditioned for another 2 min. After that, air was bubbled into to the cell and flotation was undertaken for 3 min. All flotation concentrates were filtered, dried and weighed, and the flotation recovery of anglesite or kerargyrite was calculated according to the mass obtained.

2.3 FTIR measurements

The FTIR spectra were obtained with an Nicolet model NEXUS 670 FTIR-Diffuse reflectance spectrometer which was produced by NICOLE Company, USA. About 10% (mass fraction) of the solid sample was mixed with spectroscopic grade KBr. The wave number range of these spectra was 400−4000 cm^{-1}. These spectra were recorded with 32 scans measured at 2 cm^{-1} resolution.

The samples of anglesite or kerargyrite with <2 μm particle size were first conditioned for 5 min with H_2SO_4−K_2SO_4 buffer as pH regulating reagent. Then, the samples were conditioned for another more 10 min with amyl dixanthogen. After that, solid−liquid separation was realized by centrifugal, and the solid samples were washed three times using the distilled water with the same pH value. The washed samples for FTIR analysis were dried naturally.

2.4 XRD analysis

The X-ray diffraction (XRD) patterns were recorded using a Rigaku D/MaxrA rotating anode X-ray diffractometer equipped with a Cu K_α tube and Ni filter (λ=0.1542 nm) at a scanning rate of 0.0167 (°)/s.

3 Results and discussion

3.1 Background pulp potential of zinc anode slime system

As the formula of cryptomelane can be written as $K(Mn^{4+},Mn^{2+})_8O_{16}$, or $K_2O{\cdot}15MnO_2{\cdot}MnO$, according to the stoichiometry, 93.75% of the manganese is Mn(IV) mineral. Hence, cryptomelane can be seen to have the same chemical properties as pyrolusite (MnO_2). According to the washing test on zinc anode slime, the pulp of zinc anode slime is weakly acid with pH between 1 and 5, and the concentration of Mn^{2+} is less than 3.2 g/L.

Figure 1 shows the φ−pH diagram of Mn−H_2O system [19] based on the thermodynamic calculations at 298.15 K.

As $[Mn^{2+}]$<3.2 g/L(=5.8×10^{-2} mol/L<1.0 mol/L), and as the formula for the line that represents the thermodynamic equilibrium between Mn^{2+} and MnO_2 in this figure is φ=1.229−0.02598lg$[Mn^{2+}]$−0.1183pH, the actual pulp potential of zinc anode slime will be higher than that with $[Mn^{2+}]$=1.0 mol/L. It is clear that the φ of the pulp system of zinc anode slime is mainly controlled

by the MnO_2, the concentration of Mn^{2+} and the pH in the pulp, thus forming a strong oxidation atmosphere which is called the background pulp potential of zinc anode slime. Therefore, the shadow area in the figure above the line that represents the equilibrium between Mn^{2+}($[Mn^{2+}]$=1.0 mol/L) and MnO_2 can be used as the background pulp potential of zinc anode slime.

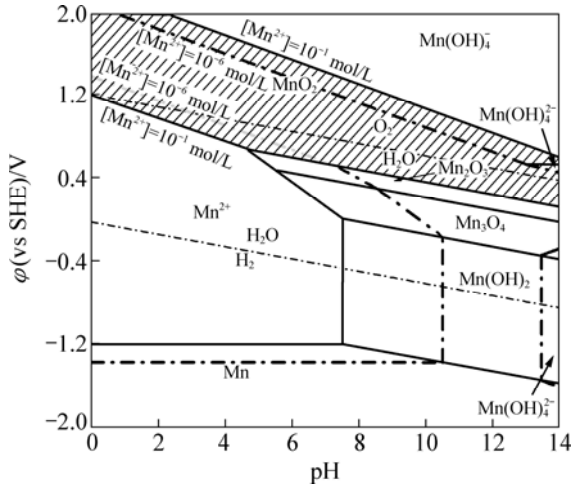

Fig. 1 φ−pH diagram of Mn−H_2O system at 298.15 K [19]

3.2 Occurrence of lead and silver in zinc anode slime

Figure 2 shows the φ−pH diagram of Pb−S−H_2O system [5] under the conditions of $[S]_T=10^{-1}$ mol/L, $[Pb^{2+}]=10^{-6}$ mol/L at 298.15 K, under the background pulp potential of zinc anode slime. As shown in Fig. 2, the vertical line at pH=1.272 represents the thermodynamic equilibrium between Pb^{2+} and $PbSO_4$. The region at the left of this line (pH<1.272) is the thermodynamic stable area of Pb^{2+}, while the region at the right side (pH>1.272) is the thermodynamic stable area of $PbSO_4$. The shadow area is the background pulp

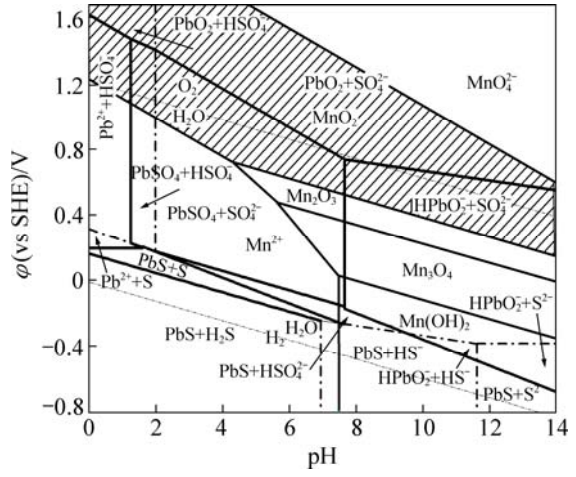

Fig. 2 φ−pH diagram of Pb−S−H_2O system under conditions of $[S]_T=10^{-1}$ mol/L and $[Pb^{2+}]=10^{-6}$ mol/L at 298.15 K, under background pulp potential of zinc anode slime

potential of zinc anode slime. It is clear that in the shadow region which represents the background pulp potential of zinc anode slime, three kinds of species, PbO_2, $PbSO_4$, and Pb^{2+}, can occur as the thermodynamic stable compounds of lead.

Figure 3 shows the φ−pH diagram of Ag−Cl−H_2O system [20] under conditions of $[Cl]_T=10^{-12}$ mol/L at 298.15 K, under the background pulp potential of zinc anode slime. As shown in Fig. 3, in the shadow region which represents the background pulp potential of zinc anode slime, elemental Ag, AgCl, Ag_2O, AgO and Ag_2O_3 can occur as the thermodynamic stable compounds of silver in acidic solution in the presence of Mn(IV) compounds.

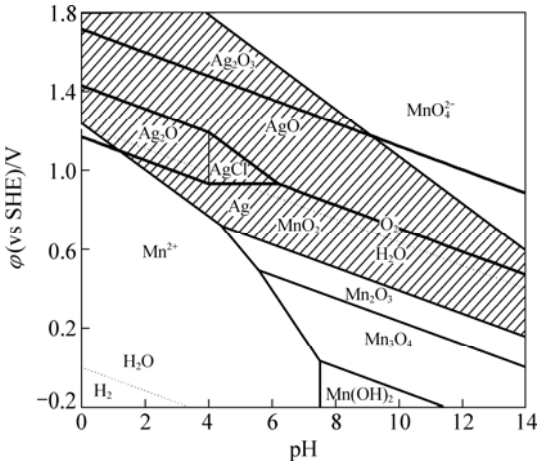

Fig. 3 φ−pH diagram of Ag−Cl−H_2O system under conditions of $[Cl^-]=10^{-12}$ mol/L at 298.15 K, under background pulp potential of zinc anode slime

Figure 4 shows the XRD pattern of zinc anode slime after removal of Mn by leaching with SO_2 as a reductant. As shown in Fig. 4, only the peaks of anglesite can be observed, so anglesite is identified as the only kind of lead mineral.

Figure 5 shows the XRD pattern of the silver flotation concentrate after removal of Mn by reductive leaching using SO_2 as a reductant. Only anglesite is identified as lead mineral. In addition, three kinds of silver minerals, kerargyrite (AgCl), silver oxide (Ag_2O_3), and silver-oxy salt Ag_7NO_{11}, are identified in the sample of Mn-removed silver concentrate of zinc anode slime.

Based on the above research and analysis, a conclusion can be drawn that anglesite ($PbSO_4$) is the only lead mineral, and kerargyrite (AgCl) is one of the silver minerals occurring in zinc electrolysis anode slime.

3.3 Occurrence of xanthate in zinc anode slime

Figure 6 shows the φ−pH diagram of butyl xanthate−H_2O system [21] under the background pulp potential of zinc anode slime. As shown in Fig. 6, in the

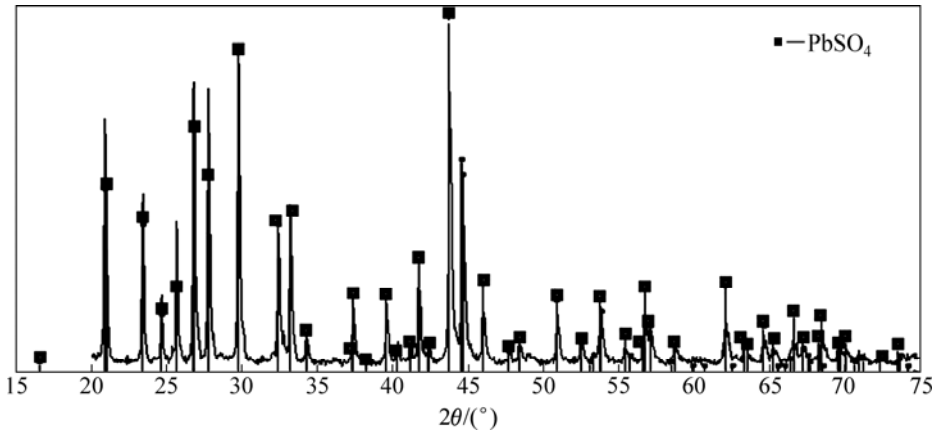

Fig. 4 XRD pattern of zinc anode slime after removal of Mn by reductive leaching with SO_2 as reductant

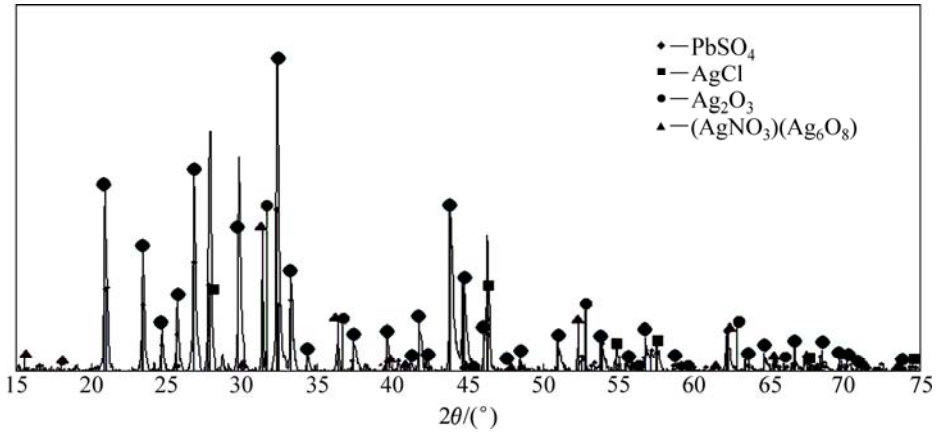

Fig. 5 XRD pattern of silver flotation concentrate after removal of Mn by reductive leaching with SO_2 as reductant

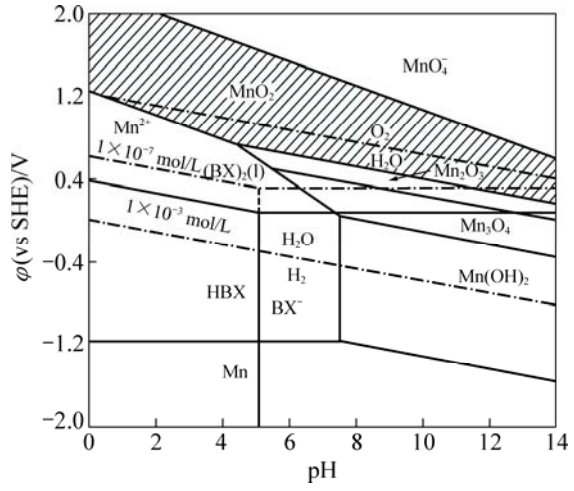

Fig. 6 φ−pH diagram of butyl xanthate−H_2O system (thin lines) under background pulp potential of zinc anode slime

shadow region that represents the background pulp potential of zinc anode slime, dixanthogen occurs as the thermodynamic stable compounds of xanthate.

3.4 Microflotation tests

Figure 7 shows the flotation result of pure kerargyrite and anglesite in sulfuric acid condition (pH=4) using amyl dixanthogen as the collector. It is clear that when the concentration of collector is larger than 5×10^{-4} mol/L, amyl dixanthogen can obtain an kerargyrite recovery rate more than 60%. However, even if the concentration of collector is increased to 1×10^{-2} mol/L, the recovery of anglesite is still less than 25%. This

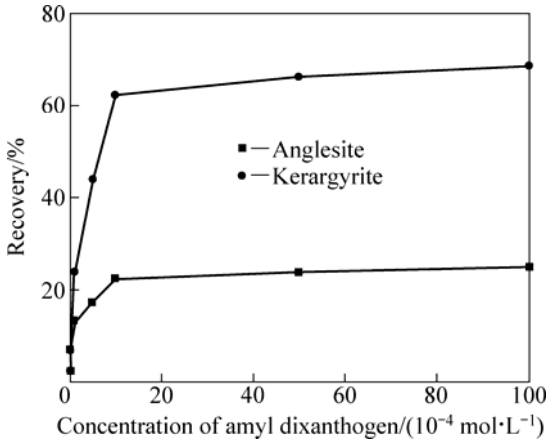

Fig. 7 Flotation result of kerargyrite and anglesite by amyl dixanthogen in sulfuric condition (pH=4)

illustrates that dixanthogen has a much stronger collecting ability to kerargyrite than to anglesite.

3.5 Molecular dynamics simulation

Molecular dynamics simulation of the adsorption of various absorbates (molecules of collectors and other coexisting ions) on the surface of absorbent (mineral) was conducted using Materials Studio. Dixanthogen, water, hydroxyl radical, sulphate and chloride were chosen as absorbates. Figure 8 shows the molecular structure of amyl dixanthogen.

Kerargyrite and anglesite were chosen as the absorbent, whose crystal structures are shown in Fig. 9.

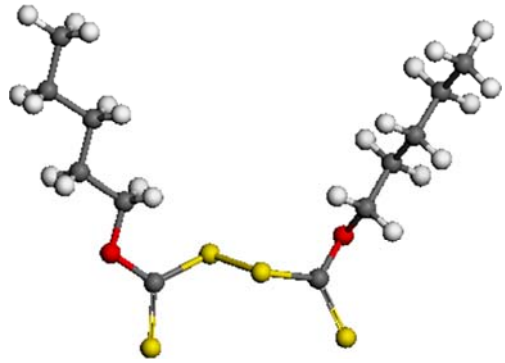

Fig. 8 Molecular structure of amyl dixanthogen

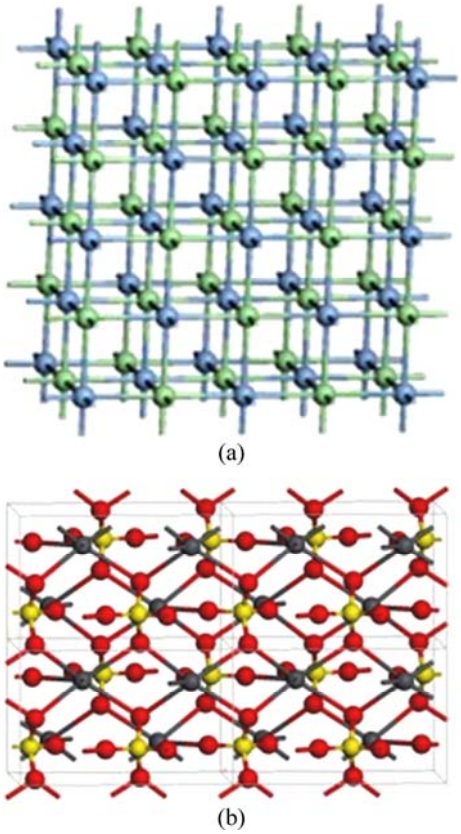

Fig. 9 Crystal structures of kerargyrite (2×2×1) (a) (Ag: Blue, Cl: Green), and anglesite (2×2×1) (b) (Pb: Dark grey, S: Yellow, O: Red)

This crystal structure was manually modeled, and the geometry optimization and charge distribution were completed using VAMP module with semi-empirical molecular orbital method. The data of mineral crystal structure were obtained from the experimental data of the inorganic crystal structure database (ICSD), and no further geometry optimization was done. The Slab Model with a vacuum layer of 50 Å to ensure that there exists enough space for absorbate molecules was established by cutting out (001) surface and extending to about 30 Å×30 Å supercell. The charge distributed on absorbent was calculated using Qeq method. The simulation of adsorption was completed by using the module of Adsorption Locator. The grand canonical ensemble Monte Carlo method was firstly used to sample the configuration space of the adsorbate-adsorbent system. Then the global minimum adsorption configuration was searched by using the simulated annealing method, and in the end, the binding energy of the adsorption was calculated.

The changes of interaction energy calculated by Material Studio (Adsorption Locater) between kerargyrite and a variety of adsorbents (dixanthogen, H_2O, OH^-, Cl^-, SO_4^{2-}) are shown in Table 1. It is clear from Table 1 that the adsorption order from strong to weak for the above adsorbents on the surface of kerargyrite is dixanthogen > H_2O > OH^- > Cl^{-1} > SO_4^{2-}. Those between anglesite and a variety of adsorbents (dixanthogen, H_2O, OH^-, Cl^-, SO_4^{2-}) are shown in Table 2. It is clear from Table 2 that the adsorption order from strong to weak for the above adsorbents on the surface of anglesite is SO_4^{2-} > dixanthogen > OH^- > H_2O > Cl^{-1}.

Table 1 Changes of interaction energy between kerargyrite and adsorbents (kJ/mol)

Species	$E_{mineral}$	$E_{collector}$	E_{total}	ΔE
Amyl dixanthogen	−173920.7	333.467	−173670.11	−82.8752
H_2O	−173920.7	302.013	−173687.65	−68.9579
OH^-	−173920.7	0.003762	−173942.38	−21.6750
SO_4^{2-}	−173920.7	−31.6802	−173959.08	−6.6968
Cl^-	−173920.7	326.326	−173550.15	44.2290

Table 2 Changes of interaction energy between anglesite and a variety of adsorbents (kJ/mol)

Species	$E_{mineral}$	$E_{collector}$	E_{total}	ΔE
Amyl dixanthogen	−258102.93	334.648	−257913.41	−145.130
H_2O	−258102.93	0.06103	−258143.88	−41.0058
OH^-	−258102.93	−35.1266	−258200.56	−62.491
SO_4^{2-}	−258102.93	312.627	−258130.84	−340.545
Cl^-	−258102.93	0.001254	−258115.72	−12.791

So a conclusion can be made that dixanthogen can be absorbed on both of the surface of kerargyrite and anglesite in the absence of SO_4^{2-}, while in the presence of SO_4^{2-}, dixanthogen can only be adsorbed on the surface of kerargyrite.

3.6 FTIR measurements

The FTIR spectra of kerargyrite and anglesite before and after interaction with amyl dixanthogen in sulphuric acidic at pH=4 are given in Fig. 10.

In the spectrum of kerargyrite after interaction with dixanthogen, the double characteristic absorption peaks of S—O—C stretching vibration in a dixanthogen molecule shifted from 1261.7 cm^{-1} and 1028.2 cm^{-1} to 1265.1 cm^{-1} and 1024.2 cm^{-1} respectively, the double characteristic absorption peaks of methylene stretching vibration and methylene asymmetric stretching vibration shifted from 2957.2 $cm^{-1}$and 2877.7 cm^{-1} to 2958.3 cm^{-1} and 2871.8 cm^{-1} respectively, and the double characteristic absorption peaks of C—S stretching vibration in a dixanthogen molecule shifted from 827.38 cm^{-1} and 689.7 cm^{-1} to 825 cm^{-1} and 691.9 cm^{-1}, respectively. A conclusion can be made from Fig. 10 that dixanthogen can be adsorbed on the surface of kerargyrite in the absence of SO_4^{2-}.

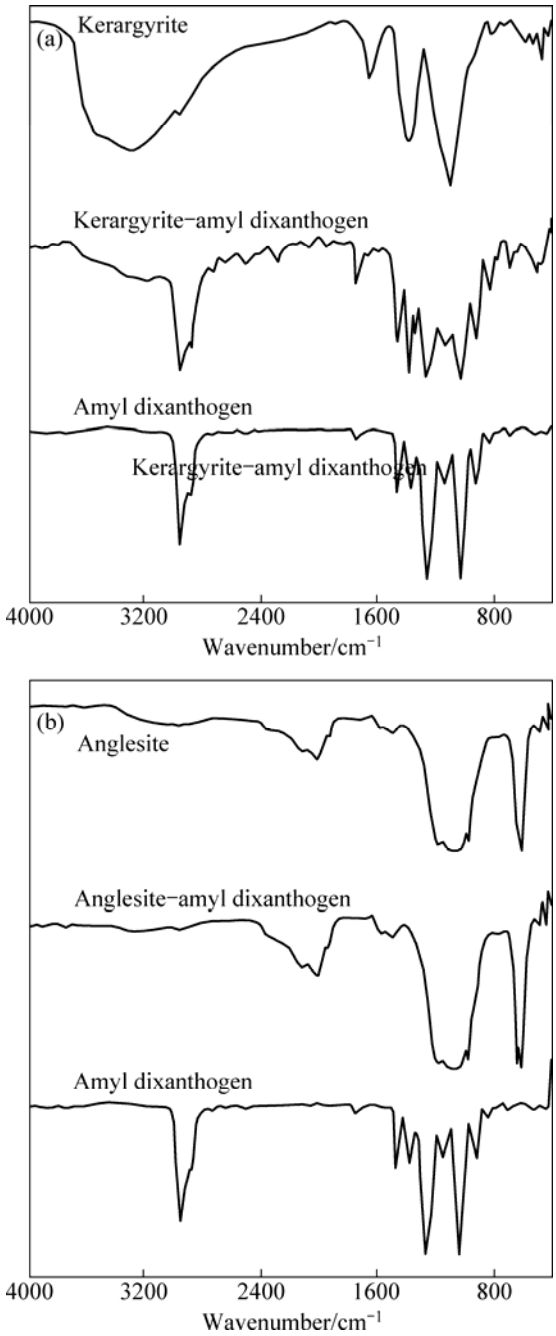

Fig. 10 FTIR spectra of kerargyrite (a) and anglesite (b) before and after their interaction with amyl dixanthogen in sulphuric acidic at pH=4

However, the situation is completely different from that in Fig. 10(b). In Fig. 10(b), in the spectrum of anglesite after interaction with dixanthogen, there don't exist the double characteristic absorption peaks of S—O—C stretching vibration in a dixanthogen molecule at 1261.7 cm^{-1} and 1028.2 cm^{-1}, the characteristic absorption peak of methylene stretching vibration in a dixanthogen molecule at 2957.2 cm^{-1}, the characteristic absorption peak of methylene asymmetric stretching vibration at 2877.7 cm^{-1}, and the characteristic absorption peaks of C—S stretching vibration in a dixanthogen molecule at 827.38 cm^{-1} and 689.7 cm^{-1}. So a conclusion can be also made that dixanthogen can be adsorbed on the surface of anglesite in the absence of SO_4^{2-}, but cannot be adsorbed on the surface of anglesite in the presence of SO_4^{2-}.

4 Conclusions

1) Thermodynamics and XRD analyses showed that anglesite is the only lead minerals, and kerargyrite is one of silver minerals occurring in zinc anode slime. The thermodynamic stable product of xanthate in the presence of Mn(IV) under acidic condition is dixanthogen.

2) Microflotation tests revealed that in sulfuric acid solution at pH=4, amyl dixanthogen has a much stronger collecting ability to kerargyrite than to anglesite.

3) The changes of interaction energy calculated by Material Studio (Adsorption Locater) between two mineral absorbents (anglesite and kerargyrite) and a variety of adsorbates (amyl dixanthogen, H_2O, OH^-, Cl^-, SO_4^{2-}) indicated that, amyl dixanthogen can be adsorbed on both of the surface of kerargyrite and anglesite in the absence of SO_4^{2-}, while in the presence of SO_4^{2-}, dixanthogen can only be adsorbed on the surface of kerargyrite.

4) The FTIR spectrum indicated that amyl dixanthogen can be selectively adsorbed on the surface of kerargyrite in the presence of SO_4^{2-}.

References

[1] TSIKLAURI O G, MARSAGISHVILI T A, TSURTSUMIYA G S, KIRILLOV S A, DZANASHVILI D I. Kinetics of anodic formation and cathodic reduction of MnO_2 in the sulfate electrolyte solutions [J]. Russian Journal of Electrochemistry, 2008, 44(11): 1299−1306.

[2] RECÉNDIZ A, NAVA J L, GONZÁLEZ I. Electrochemical characterization of MnO_2 anodically formed during the zinc electrowinning process [J]. ECS Transactions, 2008, 15(1): 79−89.

[3] YOSHIAKI U, HAJIME N, HAZUTERU T. Anodic behavior of Pb−Ag alloys in sulfuric acid solution in the presence of Cl^- or F^- [J]. Bulletin of the Research Institute of Mineral Dressing and Metallurgy, Tohoku University, 1988, 43(2): 195−204.

[4] ZHANG L. Electrochemical equilibrium diagrams for sulphidization of oxide copper minerals [J]. Minerals Engineering, 1994, 7(7): 927−932.

[5] KOBAYASHI M, KAMETANI H. The Eh−pH diagram of the Pb−S−H_2O systems and its correlation with lattice imperfection and electronic charge carriers in PbS [J]. Hydrometallurgy, 1989, 22(1−2): 141−157.

[6] WARNER T E, RICE N M, TAYLOR N. Thermodynamic stability of pentlandite and violarite and new Eh−pH diagrams for the iron−nickel sulphur aqueous system [J]. Hydrometallurgy, 1996, 41(2−3): 107−118.

[7] SILVER G L. Two predominance-region diagrams for plutonium [J]. Journal of Radioanalytical and Nuclear Chemistry, 2004, 262(3): 629−632.

[8] RASHCHI F, DASHTI A, ARABPOUR-YAZDI M, ABDIZADEH H. Anglesite flotation: A study for lead recovery from zinc leach residue [J]. Minerals Engineering, 2005, 18(2): 205−212.

[9] FUERSTENAU M C, OLIVAS S A, HERRERA-URBINA R, HAN K N. The surface characteristics and flotation behavior of anglesite and cerussite [J]. International Journal of Mineral Processing, 1987, 20(1−2): 73−85.

[10] RAO G V, SCHNEIDER F U, HOBERG H. On recovery of anglesite fines from hydrometallurgical leach residue [J]. Aufbereit Tech, 1987, 28(5): 247−254.

[11] MOHANAN P K, RAGHAVAN R, PATNAIK S C. Hydrometallurgical extraction and recovery of silver from silver concentrate generated at the zinc electrowinning plant [J]. NML Technical Journal, 1997, 39(2): 77−86.

[12] HUANG Kai-guo, WANG Qiu-feng. Recovery of silver from zinc leach residues by flotation [J]. Journal of Central South University of Technology: Natural Science, 1997, 28(6): 530−532. (in Chinese)

[13] WANG Miao-sheng, ZHENG Tuan, ZHOU Ji-gang. Study on preparation of manganese carbonate by zinc anode slime [J]. Guangzhou Research Institute of Non-Ferrous Metals, 1997, 7(2): 125−130. (in Chinese)

[14] LIAO Yun-jun, MEI Guan-gui, LIU Rong-yi. A study of reducing manganese ions impoverishment and making use of anodic slimes in zinc electrolysis [J]. China's Manganese Industry, 1999, 19(1): 30−33. (in Chinese)

[15] XIANG Ping, FENG Qi-ming, NIU Yin-jian, LIU Wei-qi. Sulphuric acid leaching of MnO_2 from zinc electrolysis anode slime using PbS as a reductant [J]. Hunan Nonferrous Metals, 2010, 26(1): 19−23. (in Chinese)

[16] XIANG Ping, FENG Qi-ming, LIU Wei-qi, LIU Lang-ming, ZHU Bei-ping, NIU Yin-jian. Leaching of MnO_2 from zinc electrolysis anode slime using SO_2 as a reductant [J]. Mine and Metallurgical Engineering, 2010, 30(8): 168−170. (in Chinese)

[17] SHEN Hui-ting, QIN Hua, HUANG Xiao-yi, BAO Xi-lin. Research on the comprehensive recovery of manganese and lead from an Mn-bearing metallurgical residue [J]. Metal Mine, 2009(6): 171−175. (in Chinese)

[18] XIANG Ping, FENG Qi-ming, LIU Lang-ming, ZHU Bei-ping, NIU Yin-jian, OU Le-ming. Beneficiation of anglesite and silver minerals from zinc electrolysis anode slime by physical method [J]. Mine and Metallurgical Engineering, 2010, 30(4): 54−57, 64. (in Chinese)

[19] SUSAN J, TEWALT, MOTOAKI SATO, DULONG F T, NEUZIL S G, ALLAN KOLKER, DENNEN K O. Use of ozone to remediate manganese from coal mine drainage waters [C]//National Meeting of the American Society of Mining and Reclamation. Breckinridge CO, 2005: 19−23.

[20] ZHONG Zhu-qian, MEI Guang-gui. Application of diagrams of chemical potential in hydrometallurgy and purification of waste water [M]. Changsha: Central South University of Technology Press, 1986. (in Chinese)

[21] SOMASUNDARAN P, WANG Dian-zuo. Solution chemistry: minerals and reagents [M]. The Netherlands: Elsevier, 2006: 220.

锌阳极泥矿浆中铅银矿物的赋存状态及其与黄药的作用

向 平[1,2]，冯其明[1]，朱阳戈[1]，邓 杰[1]，龙 涛[1]，钮因健[1]

1. 中南大学 资源加工与生物工程学院，长沙 410083；
2. 株洲市湘麒资源综合利用研究所，株洲 412005

摘 要：用热力学方法分析锌阳极泥矿浆的强氧化背景矿浆电位及其对铅、银和黄原酸盐赋存状态的影响。结果表明，在强氧化背景矿浆电位下，铅以 Pb^{2+}或 $PbSO_4$ 形式存在，银以金属银、AgCl 和 Ag_2O 等形式存在，黄原酸盐以其氧化后的二聚物双黄药形式存在。XRD 分析结果表明，锌阳极泥中的铅矿物主要是铅矾，主要的银矿物之一是氯银矿。单矿物浮选实验表明，双黄药对氯银矿的捕收力远强于对铅矾的。用 Material Studio(Adsorption Locater)模块计算了两种吸附质(铅矾和氯银矿)与不同吸附剂(双黄药, H_2O, OH^-, Cl^-, SO_4^{2-})的作用能变化。结果表明，在存在 SO_4^{2-}的条件下，双黄药只能吸附在氯银矿表面。红外光谱测试证实了双黄药对氯银矿的选择性吸附作用。

关键词：锌阳极泥；铅矾；氯银矿；黄原酸盐；吸附

(Edited by YUAN Sai-qian)